Contrib Mineral Petrol (2004) 146: 590–605
DOI 10.1007/s00410-003-0514-6

ORIGINAL PAPER

A. K. Schmitt · J. I. Simon

Boron isotopic variations in hydrous rhyolitic melts: a case study from Long Valley, California

Received: 25 November 2002 / Accepted: 11 August 2003 / Published online: 30 September 2003

Abstract In this paper, we present boron isotope analyses of variably degassed rhyolitic glasses from Long Valley, California. The following results indicate that pre-eruptive boron isotopic signatures were preserved in degassed glasses: (1) averaged secondary ionization mass spectrometry (SIMS) measurements of H_2O-rich (~3 wt%) melt inclusions from late erupted Bishop Tuff pumice are indistinguishable from positive thermal ionization mass spectrometry (PTIMS) analysis of vesiculated groundmass glass ($\delta^{11}B = +5.0 \pm 0.9‰$ and $+5.4 \pm 0.5‰$, respectively); (2) SIMS spot-analyses on H_2O-poor obsidian (~0.15 wt% H_2O) from younger Glass Mountain Dome YA (average $\delta^{11}B = +5.2 \pm 1.0‰$) overlap with compositionally similar late Bishop Tuff melt inclusions; and (3) four variably degassed obsidian samples from the 0.6 ka Mono Craters (H_2O between 0.74 and 0.10 wt%) are homogeneous with regard to boron (average $\delta^{11}B = +3.2 \pm 0.8‰$, MSWD = 0.4). Insignificant variations in $\delta^{11}B$ between early and late Bishop Tuff melt inclusion glasses agree with published experimental data that predict minor ^{11}B depletion in hydrous melts undergoing gas-saturated fractional crystallization. Melt inclusions from two crystal-rich post-caldera lavas (Deer Mountain and South Deadman Dome) are comparatively boron-rich (max. 90 ppm B) and have lower $\delta^{11}B$ values (average $\delta^{11}B = +2.2 \pm 0.8‰$ and -0.4 ± 1.0 ‰) that are in strong contrast to the boron isotopic composition of post-caldera crystal-poor rhyolites (27 ppm B; $\delta^{11}B = +5.7 \pm 0.8‰$). These variations in $\delta^{11}B$ are too large to be caused by pre-eruptive degassing. Instead, we favor assimilation of ^{11}B depleted low-temperature hydrothermally altered intrusive rocks subsequent to fresh rhyolite recharge.

Editorial responsibility: J. Hoefs

A. K. Schmitt (✉) · J. I. Simon
Department of Earth and Space Sciences,
University of California Los Angeles,
Los Angeles, CA, 90095-1567 USA
E-mail: axelk@gfz-potsdam.de
Tel.: +49-0331-2881423
Fax: +49-0331-2881474

A. K. Schmitt
Sektion 4.2 Anorganische und Isotopen-Geochemie,
GeoForschungsZentrum Potsdam,
Telegrafenberg B123, 14473 Potsdam, Germany

Introduction

One of the main applications of stable isotope geochemistry in igneous petrology is to identify the roles of different source components during magmagenesis. For example, boron isotopes were successfully applied to trace crustal components in subduction-related basaltic and andesitic rocks (e.g., Palmer 1991; Ishikawa and Nakamura 1994; Rose et al. 2001). This approach is based on the strong boron isotopic fractionation between fluids and silicates, which is controlled by the relative partitioning of ^{11}B and ^{10}B between trigonally and tetragonally coordinated species (e.g., Palmer and Swihart 1996). Boron isotopic fractionation is particularly effective at the lithosphere-hydrosphere interface, where rocks interact with low-temperature fluids such as seawater or meteoric waters (e.g., Spivack and Edmond 1987). For continental geothermal systems, hydrothermal waters are commonly ^{11}B enriched compared to their local volcanic host rocks (Palmer and Sturchio 1990; Palmer and Swihart 1996; Schmitt et al. 2002) whereas secondary hydrothermal silicates will preferentially incorporate ^{10}B (e.g., Hervig et al. 2002). Hydrothermally overprinted rhyolites from Yellowstone caldera are indeed depleted in ^{11}B by almost $-5‰$ compared to unaltered equivalents (Palmer and Sturchio 1990). Thus, boron isotopes can potentially reveal remelting or assimilation of hydrothermally altered but otherwise chemically similar rocks, and might therefore be complementary to evidence from low-^{18}O magmas (e.g., Bacon et al. 1989). Furthermore, hydrous fluids also play an important role in high-temperature magmatic processes, but little is known, for example,

about the effects of boron isotope fractionation in natural volatile-saturated melts despite experimental evidence for measurable fractionation at elevated temperatures (Hervig et al. 2002).

Long Valley caldera, located in central California (Fig. 1), is ideal to explore the boron isotope systematics of hydrous rhyolitic melts. This is due to its youthfulness, accessibility, and extensive eruptive record that encompasses end-member styles of silicic volcanism: (1) large-volume ignimbrites that tapped a continuously viable, but compositionally and thermally zoned magma chamber (e.g., Hildreth et al. 1979) and (2) small-volume, texturally and compositionally contrasting lavas that apparently had a long history of pre-eruptive crystallization, magma storage and thermal rejuvenation (e.g., Sampson and Cameron 1987; Reid et al. 1997). Based on published maps, stratigraphy, and nomenclature, we sampled pumice from early and late erupted portions of the $\sim$600 km^3 Bishop Tuff (Wilson and Hildreth 1997) and lavas from small-volume ($\sim$0.5 km^3; Miller 1985) post-caldera domes (Deer Mountain and South Deadman Dome; Bailey 1989). While a comprehensive view of boron isotopic variations in the Long Valley magma system over its $>$2-Ma life-span is beyond the purpose of this paper, we include a cursory exploration of pre-caldera Glass Mountain Domes and other Inyo-Mono Domes for comparison.

We demonstrate that magmatic boron isotope signatures remain largely unchanged during eruptive degassing. We further propose that degassing and post-eruptive alteration can be dismissed to explain the observed $\sim$8‰ variations in δ^{11}B in Long Valley rhyolitic glasses. Instead, we favor open-system mixing-assimilation processes. Because crustal contamination by local country rocks is inconsistent with trace element compositions of melt inclusions in post-caldera rhyolites, this leaves assimilation of ^{11}B depleted hydrothermally altered precursor intrusions as a geologically plausible alternative.

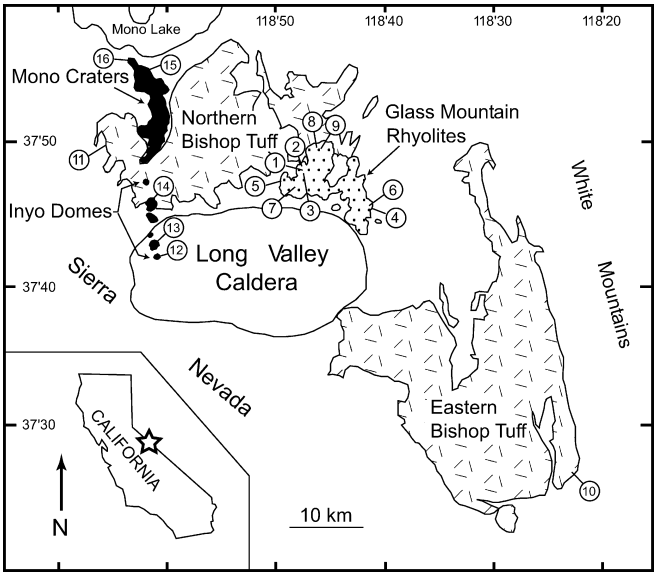

Fig. 1 Map of the Long Valley caldera and Glass Mountain showing distribution of Bishop Tuff and sampling locations for this study (after Wilson and Hildreth 1997). *1* OC (MR01LV61), *2* OC (MR01LV60), *3* OC (JS01LV01), *4* OL (JS01LV05), *5* OD (MR01LV63), *6* YO (JS01LV06), *7* YG (MR01LV62), *8* YA (JS01LV04), *9* YA (JS01LV03), *10* Early Bishop Tuff (BT01), *11* Late Bishop Tuff (BT02), *12* Deer Mountain (IN02), *13* South Deadman Dome (IN01), *14* Obsidian Dome (ObD01), *15* Upper Dome, *16* Panum Dome (including MC84 samples)

Geological background

Approximately 1,600 references of previous geoscientific research pertaining to Long Valley and vicinity are listed in Ewert and Harpel (2000). Here, we briefly summarize only those studies that guided our sample selection by providing a conceptual framework for the still controversially discussed magmatic processes. The 0.76-Ma (Sarna Wojcicki et al. 2000) Bishop Tuff presently outcrops radially east to southeast and north of the Long Valley caldera (Fig. 1; Rinehart and Ross 1957; Wilson and Hildreth 1997). The caldera is located on the eastern flank of the Sierra Nevada at the western boundary of the extensional Basin and Range Province. Jurassic and Cretaceous granitoids of the Sierra Nevada batholith largely make up the country rock (Rinehart and Ross 1957). Bishop Tuff is a high-Si rhyolite zoned in composition and mineralogy (Hildreth 1979, 1981; Wallace et al. 1995, 1999). Close similarity in O, Sr, Nd, and Pb isotopic ratios for early and late erupted portions of the Bishop Tuff (e.g., Halliday et al. 1984; Davies and Halliday 1998; Bindeman and Valley 2001) is consistent with near-eutectic fractional crystallization within a continuously viable magma body. There are, however, indications for a more complicated magmagenesis. For example, feldspar populations in early-erupted Bishop Tuff are heterogeneous in their Sr and Nd isotopic composition (Davies and Halliday 1998). In addition, inverse phenocryst zonations and less-evolved melt inclusions near crystal rims in late Bishop Tuff imply magma mixing or crystal sinking (Dunbar and Hervig 1992; Anderson et al. 2000).

The northeast margin of Long Valley caldera intersects the 2.1–0.79-Ma high-Si rhyolites of Glass Mountain, a complex of lava domes and flows intercalated with pyroclastic material (Metz and Mahood 1984, 1985; Metz and Bailey 1993). Trace element compositions as well as Sr, Nd, and Pb isotopic ratios of younger Glass Mountain rhyolites are smaler to those of Bishop Tuff and therefore, it has been debated whether they originated from the same persistent body of magma that eventually produced the caldera-forming eruption of the Bishop Tuff (Halliday et al. 1989; Sparks et al. 1990; Mahood 1990; Metz and Mahood 1991; Metz and Bailey 1993; Christensen and DePaolo 1993; Davies et al. 1994; Davies and Halliday 1998). ^{40}Ar/^{39}Ar (van den Bogaard and Schirnick 1995) and Rb-Sr (Christensen

and Halliday 1996) model ages for melt inclusion bearing quartz crystals from Bishop Tuff supported the presence of a long-lived (~1.1 and >0.3 Ma, respectively) magma body. In contrast, U-Pb zircon ages for the early-erupted Bishop Tuff (Reid and Coath 2000) suggested much shorter magma residence times (<0.1 Ma).

Subsequent to the climactic Bishop Tuff eruption, the Long Valley magma system continued to produce predominately rhyolitic eruptives between 750 and 650 ka that formed a resurgent dome (Bailey et al. 1976). After a hiatus of ~100 ka, three groups of crystal-rich moat rhyolites erupted at ~200-ka intervals including the ~100-ka Deer Mountain Dome (Heumann and Davies 1997; Heumann et al. 2002).

The most recent eruptions associated with Long Valley formed the Inyo Domes, a chain of mainly ~0.6-ka domes and flows that extend from the northwest corner of the caldera to the south end of the Mono chain (Fig. 1; Miller 1985; Sieh and Bursik 1986). While a finely porphyritic (FP) lava type dominates north of the caldera rim, intra-caldera domes consist of intermingled FP and coarsely porphyritic (CP) lavas (e.g., South Deadman Dome; Bailey et al. 1976; Sampson 1987; Sampson and Cameron 1987; Vogel et al. 1989). By contrast, coeval high-Si rhyolites erupted from Mono Craters (~0.6 ka; Sieh and Bursik 1986) are largely aphyric (Kelleher and Cameron 1990). Sampson and Cameron (1987) argued that textural heterogeneities, thermal and compositional discontinuities indicate isolated magma systems for FP and CP lavas, whereas Inyo FP and Mono high-Si rhyolites might be genetically related (Kelleher and Cameron 1990). The well-defined Pb-Sr isotope mixing line that includes resurgent dome rhyolites, crystal-rich moat rhyolites, and Inyo Domes might further indicate some genetic relation between these suites of post-caldera rhyolites (Heumann and Davies 1997). ^{230}Th-^{238}U zircon ages for Deer Mountain and South Deadman Dome overlap despite a difference in eruption ages of ~100 ka, which suggests protracted magma storage or recycling of earlier formed crystals (Reid et al. 1997).

Sample selection, preparation and analysis

Melt inclusions

We studied quartz-hosted melt inclusions from 'early' (BT01) and 'late' (BT02) erupted pumice from basal (F6 fall deposit) and upper parts in the Bishop Tuff sequence (Ig2NWb), respectively. Melt inclusion bearing quartz crystals were further separated from South Deadman Dome CP lava (IN01) and Deer Mountain crystal-rich lava (IN02). Quartz phenocrysts (1 to 2 mm in diameter) were handpicked after a gentle crushing of the rocks and individually mounted in epoxy. Glassy, undevitrified inclusions were exposed on both sides by grinding and polishing (final polish with 0.3 μm Al_2O_3). For ion microprobe analysis, approximately ten crystals per each sample were epoxy-mounted in 3-mm holes drilled into 1-in Al-disks that also contained a polished fragment of NIST SRM 610 reference glass. All inclusions inspected in pumice from late Bishop Tuff (BT02) were opaque due to strong devitrification. After heating melt inclusion bearing quartz crystals in an Au-capsule (at 100 MPa and 800 °C for 24 h), many inclusions became glassy and appear to be homogeneous. These were selected and further treated in the same manner as unheated samples.

Obsidian glasses

Eight crystal-poor obsidians from the pre-caldera Glass Mountain complex were included in this study. Overall, our sampling of older and younger Glass Mountain Domes (three samples each) represents the geographical extent of the Glass Mountain volcanic complex and the range of eruption ages (Fig. 1). To test for intra-flow homogeneity, Dome OC and Dome YA were sampled in three and two different locations, respectively (Fig. 1). FP lava was sampled from Obsidian Dome (ObD01) and South Deadman Dome (IN01G) adjacent to CP lava used for separation of melt inclusion bearing quartz. Four fragments of coeval Mono Craters dome and block-and-ash flow lavas were further selected. They exhibit various degrees of eruptive degassing that is indicated by a ~50‰ decrease in δD with concomitant decrease in H_2O abundance from ~0.8 to 0.1 wt% (Newman et al. 1988). All samples were dense, unvesiculated obsidians. Fragments (~1 mm in diameter) were broken from the interior of hand-specimens and embedded in epoxy. Polishing and further sample treatment followed in the same way as described for the melt inclusion samples.

Bulk glass separate

Approximately 100 mg of glassy groundmass fragments were hand-picked from gently crushed BT02 pumice that was also used for separation of melt inclusion bearing quartz. Glass fragments (~0.5 mm) were inspected for absence of phenocrysts under a binocular microscope. The separate was ultrasonically cleaned for 2 min in deionized water in order to remove any dissolvable surface contamination, dried at 105 °C overnight, and then grinded in an agate mortar and digested following methods described in Kasemann et al. (2002).

Analytical

Boron isotopes in the bulk glass separate were analyzed by positive thermal ionization mass spectrometry (PTIMS) at the GeoForschungsZentrum Potsdam (GFZ) following techniques described in Kasemann et al. (2002). Glass analyses by secondary ionization mass spectrometry (SIMS) were performed using the CAMECA

IMS1270 ion microprobe at the University of California, Los Angeles (UCLA). $^{11}B^+$ and $^{10}B^+$ secondary ions were measured by bombarding a ~25-μm spot of the sample surface with a ~20-nA and 22.5-keV $^{16}O^-$ primary ion beam. A 3-min pre-sputtering was applied to reduce surface contamination. The secondary acceleration potential was 10 keV and the energy bandpass was set to 50 eV. The mass resolution was tuned to ~1,800, sufficient to resolve mass interferences of $^9Be^1H^+$ and $^{10}B^1H^+$. $^{11}B^+$ and $^{10}B^+$ ions were collected in a single electron multiplier in peak switching mode with counting times on $^{11}B^+$ and $^{10}B^+$ of 5 and 10 s per cycle, respectively. Deadtime-corrected (25 ns) and drift-corrected ratios of $^{11}B^+/^{10}B^+$ were then calculated from 15 to 50 cycles per analysis. Instrumental mass fractionation ($\beta = (^{11}B/^{10}B)_{measured}/(^{11}B/^{10}B)_{true}$) was determined for each analytical session by interspersed analyses of NIST SRM 610 glass with $\delta^{11}B = -1.05 \pm 0.80‰$ (Kasemann et al. 2002; all values relative to NIST SRM 951 standard boric acid with $^{11}B/^{10}B = 4.04558$; 1 standard deviation computed from individual independent measurements). During a 9-month period, β varied by about 10‰ (between 0.9596 and 0.9695), likely due to differences in secondary ion steering and/or gain of the electron multiplier.

Subsequent to the completion of boron isotope measurements, the instrument was retuned to low mass resolution (500) and boron and selected trace elements were analyzed with a small (~10 μm) $^{16}O^-$-beam in the same analysis spot (Fig. 2). Energy filtering was applied to suppress molecular interferences (−100 V offset) and measured intensities were normalized to $^{30}Si^+$. Concentrations were computed using relative sensitivity factors determined from interspersed analysis of NIST SRM 610 (Table 1). Based on the external reproducibility on NIST SRM 610 and counting statistics of unknowns, we estimate relative uncertainties in trace element concentrations to be better than ~5% for Li and B, and < 10% for other trace elements (Table 1).

We imaged glasses to assess sample homogeneity (Fig. 2) using a Leo 1430VP scanning electron microscope (UCLA) and determined major element compositions by electron microprobe analysis using CAMECA SX-100 instruments at the GFZ and the Australian National University (ANU), Canberra. In order to verify preservation of pre-eruptive volatiles in melt inclusion glasses, H_2O and CO_2 were analyzed by Fourier-transformed infrared spectroscopy (GFZ, ANU) following the technique described in Wallace et al. (1999).

Results

Major and trace element compositions

Most glasses analyzed were high-Si rhyolites with SiO_2 contents typically between ~75 and ~79 wt% (all normalized to 100 wt% anhydrous; Table 2). Melt inclusion glasses from early and late Bishop Tuff and South Deadman Dome CP lava have indistinguishable and largely invariant major element compositions typical for near-eutectic crystallization. Compared to the former, most Deer Mountain melt inclusions are characterized by slightly lower CaO, and somewhat higher Al_2O_3 and Fe_2O_3 contents (Table 2). Glasses from crystal-poor FP lavas (South Deadman Dome and Obsidian Dome) have lower SiO_2 contents (~72 and ~74 wt%, respectively) that closely overlap with respective whole-rock compositions (Sampson and Cameron 1987). In contrast, strong differences between whole-rock and glass compositions exist for crystal-rich lavas. For example, SiO_2 contents in melt inclusions from CP lavas of South Deadman Dome are much higher (78.1 wt%) than reported for whole-rocks or even groundmass glass separates (71.5 and 75.8 wt%, respectively; Sampson and Cameron 1987). Similar differences occur for trace elements that tend to be highly enriched in (micro-)phenocrysts such as plagioclase (Fig. 2) or accessory phases such as allanite and zircon. As an example, Table 1 summarizes strongly divergent whole-rock and glass compositions for FP rhyolite, in particular for the feldspar compatible elements Sr and Ba. There is, however, good agreement for incompatible trace elements (e.g., Rb) and boron between undevitrified whole-rock samples (Higgins 1988) and glass analyses (Table 1).

In Fig. 3 we explore trace element variations vs. boron for melt inclusions from Bishop Tuff and post-caldera lavas. For the Bishop Tuff, melt inclusion compositions from two individual pumice clasts are tightly grouped and closely match the field defined by the Anderson et al (2000) data which incorporated approximately five times more analyses from a stratigraphically comprehensive sample set (Fig. 3). In both sets of data, fluid-immobile incompatible trace elements (e.g., Y, Nb, and Th; Strurchio et al. 1986) correlate with B, whereas feldspar-compatible trace elements such as Sr and Ba display inverse trends. These observations also hold for post-caldera dome inclusions, but absolute abundances and slopes of inter-element trends are clearly different (Fig. 3).

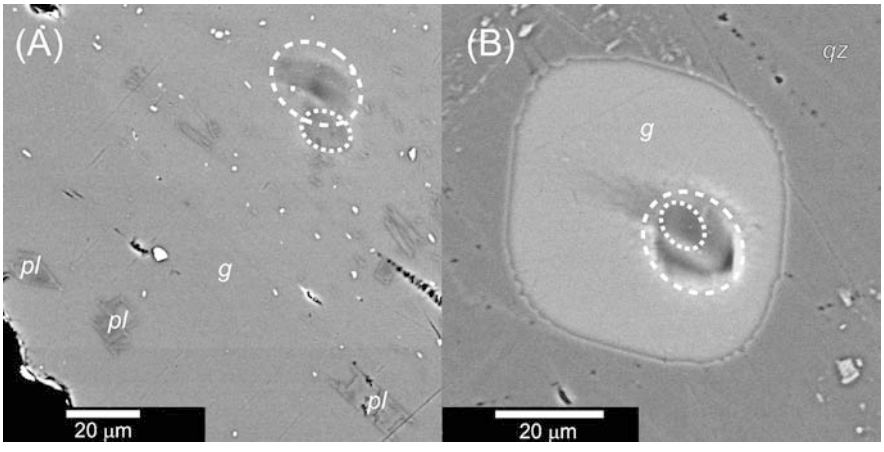

Fig. 2 Backscattered electron microscope images of (**A**) finely porphyritic (FP) rhyolite (IN01G) and (**B**) melt inclusion glass (*g*) hosted in quartz (*qz*) from coarsely porphyritic (CP) rhyolite (IN01). The sample was collected at the eastern margin of South Deadman Dome, where both lava types occur closely intermingled. *White lines* indicate ion microprobe craters for boron isotope (*dashed*) and trace element measurements (*dotted*). Note skeletal growth of plagioclase (*pl*) crystallites in FP glass (*g*) that probably represent quench crystals

Table 1 Example of relative sensitivity factors for ion microprobe trace element analysis determined on NIST 610 glass and comparison between reference values and ion microprobe results for natural and synthetic rhyolitic glasses (Chaussidon et al. 1997; M. Chaussidon, personal communication; Lindsay et al. 2001; Vogel et al. 1989; Sampson and Cameron 1987; Higgins 1988). Note good agreement between ion microprobe boron analyses with data presented by Higgins (1988) for undevitrified Obsidian Dome glass. Ion microprobe glass analyses (Toconao and Obsidian Dome) are typically lower compared to whole-rock analyses for trace elements that are hosted by feldspar (Sr, Ba) or accessory zircon (Y, Zr, Hf, U)

	NIST SRM 610				GB4				Toconao pumice				Obsidian Dome FP		
	Reference[a]		Rsf[b]		Reference[c]		Measured		Reference[d]		Measured		Reference[e,f]		Measured
	Abund. (wt%)	±1 SD	Average	±1 SD	Average (wt%)	±1 SD	Average	±1 SD	Min. (wt%)	Max.	Average	±1 SD	Min. (wt%)	Max.	
SiO_2	70.0				77.9				74.0	75.0	73.6	0.7	70.1	74.0	73.9
$\delta^{11}B$	−0.05	0.80			−12.9		−13.3	1.2							
	(ppm)				(ppm)		(ppm)		(ppm)		(ppm)		(ppm)		(ppm)
Li	484.6	21.7	0.04892	0.00274	384	-	385	6.7	-		-	-	-		
B	356.4	7.3	0.00992	0.00048	970	-	963	25	-		-	-	27.0	28.7	29
Rb	431.1	11.4	0.00104	0.00005	-	-	-	-	214	223	216	8.1	127	156	133
Sr	497.4	18.3	0.00405	0.00023	-	-	-	-	37	49	38	5.7	40	211	19
Y	449.9	19.3	0.00547	0.00022	-	-	-	-	26	28	22	1.0	25	28	22
Zr	439.9	7.8	0.00215	0.00011	-	-	-	-	57	75	52	4.4	243	357	199
Nb	430.8	37.5	0.00262	0.00015	-	-	-	-	19	20	18	0.8	21	22	16
Ba	424.1	29.3	0.00161	0.00012	-	-	-	-	532	700	625	129	386	1196	144
La	457.4	72.4	0.00261	0.00016	-	-	-	-	14		15	1.1	73.7	76.8	70
Nd	430.8	37.5	0.00079	0.00006	-	-	-	-	-	-	-	-	39.9	43.9	33
Hf	417.7	28.2	0.00049	0.00004	-	-	-	-	-	-	-	-	7.1	7.3	6.5
Th	450.6	27.8	0.00108	0.00007	-	-	-	-	16		13	2.2	20.9	21.6	18
U	457.1	13.8	0.00096	0.00008	-	-	-	-	8.1		7.0	0.5	5.5	6.6	4.2

[a]Pearce et al. (1995); Kasemann et al. (2002)
[b]Relative sensitivity factor $RSF = (X^+/^{30}Si^+)/([SiO_2]/[X])$
[c]Chaussidon et al. (1997); Chaussidon (personal communication)
[d]Lindsay et al. (2001)
[e]SiO_2 from Vogel et al. (1989)
[f]Rb, Sr, Y, Zr, Nb and Ba from Sampson and Cameron (1987); B and other traces from Higgins (1988); B in devitrified obsidian between 10.7 and 22.7 ppm

Li contents typically vary much stronger compared to B (Fig. 4). We find some melt inclusion glasses including one hourglass inclusion (inclusion connected to the matrix glass) with extremely low Li concentrations (< 10 ppm). Previous authors (e.g., Dunbar and Hervig 1992) reported similar observations. Despite occasional erratic depletions in Li contents, there appears to be a clear gap between early and late inclusions that might indicate some discontinuity within the Bishop magma system (Fig. 4A–F). Also note opposite slopes for trace element vs. Li trends in Bishop Tuff and post-caldera domes melt inclusions (e.g., Fig. 4B, H). This contrasting behavior of Li is remarkable given the close chemical similarity between both suites of high-Si rhyolites.

Volatile components in glasses

Late Bishop Tuff melt inclusions have average H_2O contents of 2.9 ± 0.4 wt% (2 SE) that are lower compared to early Bishop Tuff melt inclusions (4.4 ± 0.5 wt% H_2O). Average H_2O contents in melt inclusions from Deer Mountain (4.5 ± 0.5 wt%) and South Deadman Dome CP lava (3.9 ± 0.6 wt%) overlap with early Bishop Tuff values (Fig. 3). Results for Bishop Tuff melt inclusions agree closely with H_2O measurements reported by Dunbar and Hervig (1992), but are ~15–25% lower than average values in Anderson et al. (2000), in particular for late Bishop Tuff (Fig. 3). Although we cannot rule out some H_2O loss due to furnace treatment of BT02 quartz, this appears unlikely in the light of Anderson et al.'s (2000) results that found no discernible effects of laboratory heating on melt inclusion H_2O contents. In this context, it is noteworthy that South Deadman Dome melt inclusions preserved high H_2O contents despite the fact that their CP host lava is intermingled with strongly degassed FP lava (Table 2). High H_2O contents suggest that quartz effectively shielded the melt inclusions and that diffusive degassing during the eruption was insignificant despite relatively high temperatures of the intermingled FP magma (~925 °C; Vogel et al. 1989).

CO_2 contents up to ~300 ppm were detected in late Bishop Tuff inclusions, but for other units CO_2 was typically between 10 and 100 ppm or below the detection limit (Table 2). Obsidian glasses have low H_2O (0.1–0.8 wt%) and CO_2 (< 5 ppm) abundances, consistent with effective degassing during magma ascent and emplacement (Table 2). Our results for Mono Crater obsidians (Table 2) agree well with H_2O abundances reported by Newman et al. (1988). Note that for aliquots of the same samples, Newman et al. (1988) measured δD

Table 2 Major element, volatile, trace element and boron isotopic compositions of Long Valley rhyolite glasses. See section for description of analytical techniques. Zircon saturation temperatures computed according to Watson and Harrison (1983). Gas-saturation pressures calculated using software by Newman and Lowenstern (2002)

Sample number	Unit	Crystal-inclusion	SiO_2 (wt%)	TiO_2 (wt%)	Al_2O_3 (wt%)	Fe_2O_3 (wt%)	MnO (wt%)	MgO (wt%)	CaO (wt%)	K_2O (wt%)	Na_2O (wt%)	P_2O5 (wt%)	Total oxides (wt%)	H_2O (wt%)	CO_2 (ppm)	Li (ppm)	B (ppm)	Rb (ppm)	Sr (ppm)	Y (ppm)	Zr (ppm)	Nb (ppm)	Ba (ppm)	La (ppm)	Nd (ppm)	Hf (ppm)	Th (ppm)	U (ppm)	δ^{11}B	T ZrP (°C)	sat (MPa)
Older Glass Mountain matrix glasses[a]																															
MR01LV61	OC	1														130	95	273	0.22	35	92	51	0.6	15	15	4.7	23	12	4.2	-	-
MR01LV61	OC	2														-	-	281	0.21	36	81	50	0.7	14	20	3.8	24	9.8	5.7	-	-
MR01LV61	OC	3														-	-	275	0.32	36	84	50	0.9	14	16	5.1	20	9.8	4.7	-	-
MR01LV60	OC	1														109	103	312	0.06	38	87	58	0.5	16	18	7.2	32	16	3.9	-	-
MR01LV60	OC	2														-	-	-	-	-	-	-	-	-	-	-	-	-	3.4	-	-
MR01LV60	OC	3														-	-	-	-	-	-	-	-	-	-	-	-	-	2.9	-	-
JS01LV01	OC	1	77.2	0.06	12.8	0.62	0.11	0.01	0.32	4.41	4.49	0.02	100.3	0.19	b.d.	121	95	248	0.09	35	83	51	0.3	14	15	5.4	23	11	7.5	733	-
JS01LV01	OC	2														-	-	-	-	-	-	-	-	-	-	-	-	-	6.5	-	-
JS01LV01	OC	3														-	-	-	-	-	-	-	-	-	-	-	-	-	5.2	-	-
JS01LV05	OL	1														93	76	223	0.43	27	77	37	0.3	15	14	4.7	14	7.2	4.9	-	-
JS01LV05	OL	2														-	-	-	-	-	-	-	-	-	-	-	-	-	6.0	-	-
JS01LV05	OL	3														88	70	191	0.10	27	75	35	0.3	14	16	4.3	16	7.6	6.7	-	-
JS01LV05	OL	4														-	-	-	-	-	-	-	-	-	-	-	-	-	5.7	-	-
JS01LV05	OL	5														-	-	-	-	-	-	-	-	-	-	-	-	-	4.1	-	-
JS01LV05	OL	6														-	-	-	-	-	-	-	-	-	-	-	-	-	5.2	-	-
MR01LV63	OD	1														-	116	267	0.28	40	74	44	0.6	10	14	6.3	29	12	6.2	-	-
MR01LV63	OD	2														-	-	256	0.51	38	72	44	0.4	10	13	7.1	25	9.3	4.4	-	-
MR01LV63	OD	3														121	111	269	0.43	36	77	45	0.3	9.3	12	4.9	28	10	3.7	-	-
MR01LV63	OD	4														100	109	292	0.37	36	80	49	0.4	10	15	6.5	31	13	5.4	-	-
MR01LV63	OD	5														-	-	-	-	-	-	-	-	-	-	-	-	-	5.4	-	-
MR01LV63	OD	6														-	-	-	-	-	-	-	-	-	-	-	-	-	5.7	-	-
Younger Glass Mountain matrix glasses[a]																															
JS01LV06	YO	1														64	53	146	1.0	21	70	20	1.5	19	15	4.2	13	5.2	10.3	-	-
JS01LV06	YO	2														-	-	-	-	-	-	-	-	-	-	-	-	-	8.5	-	-
JS01LV06	YO	3														-	-	-	-	-	-	-	-	-	-	-	-	-	8.8	-	-
JS01LV06	YO	4														-	-	-	-	-	-	-	-	-	-	-	-	-	7.2	-	-
JS01LV06	YO	5														-	-	-	-	-	-	-	-	-	-	-	-	-	7.8	-	-
MR01LV62	YG	1														55	51	141	1.8	19	64	19	4.7	21	15	3.5	16	4.3	5.4	-	-
MR01LV62	YG	2														-	-	-	-	-	-	-	-	-	-	-	-	-	3.4	-	-
MR01LV62	YG	3														-	-	-	-	-	-	-	-	-	-	-	-	-	4.4	-	-
JS01LV04	YA	1														58	49	134	2.5	19	80	19	5.4	32	20	3.5	19	5.4	5.4	-	-
JS01LV04	YA	2														-	-	-	-	-	-	-	-	-	-	-	-	-	4.2	-	-
JS01LV04	YA	3														-	-	-	-	-	-	-	-	-	-	-	-	-	4.9	-	-
JS01LV03	YA	1	77.3	0.08	12.7	0.71	0.03	0.05	0.45	4.84	3.89	0.01	100.3	0.15	b.d.	54	47	126	2.2	18	75	17	4.9	27	16	3.2	15	4.8	5.2	727	-
JS01LV03	YA	2														-	-	-	-	-	-	-	-	-	-	-	-	-	6.7	-	-
JS01LV03	YA	3														-	-	-	-	-	-	-	-	-	-	-	-	-	5.2	-	-
Early Bishop Tuff melt inclusion glasses[b]																															
BT01	F6	1-1	78.8	0.03	12.7	0.64	0.03	0.01	0.44	5.31	2.02	b.d.	92.4	4.7	42	6.2	62	183	1.1	17	63	19	0.7	15	12	3.5	15	4.3	0.3	734	126
BT01	F6	3-1	78.8	0.09	12.5	0.72	b.d.	0.05	0.44	4.71	2.70	0.01	92.3	3.6	6	66	57	158	1.6	19	63	20	1.8	14	10	3.1	19	6.9	3.7	730	74
BT01	F6	4-1	78.9	0.08	12.5	0.74	b.d.	0.03	0.50	4.36	2.88	b.d.	93.1	3.2	b.d.	64	58	161	1.2	18	72	19	1.7	17	13	5.0	17	8.0	2.6	740	59
BT01	F6	5-1	78.2	0.05	12.4	0.86	0.06	0.03	0.50	4.49	3.33	0.01	93.7	4.4	33	64	58	161	1.2	18	72	19	1.7	17	13	5.0	17	8.0	4.4	733	111
BT01	F6	6-1	78.3	0.03	12.3	0.71	0.04	0.02	0.44	4.54	3.62	0.02	92.6	4.1	b.d.	78	64	156	1.9	18	61	18	1.4	16	12	1.6	18	7.3	3.7	715	93
BT01	F6	8-1	77.9	0.10	12.5	0.75	0.06	0.04	0.46	4.60	3.54	0.01	93.5	4.2	78	66	57	147	1.4	17	65	17	1.1	15	10	1.9	16	4.9	3.7	722	97
BT01	F6	9-1	78.1	0.10	12.5	0.77	0.04	0.03	0.46	4.58	3.46	0.03	93.6	6.0	37	76	63	168	1.6	20	73	20	2.4	17	12	3.5	20	8.8	4.4	732	190
BT01	F6	9-2 hg	-	-	-	-	-	-	-	-	-	-	-	-	-	8.9	67	188	1.9	18	64	20	1.7	14	12	2.4	17	8.0	2.4	-	-

Table 2 (Contd.)

Sample number	Unit	Crystal-inclusion	SiO_2 (wt%)	TiO_2 (wt%)	Al_2O_3 (wt%)	Fe_2O_3 (wt%)	MnO (wt%)	MgO (wt%)	CaO (wt%)	K_2O (wt%)	Na_2O (wt%)	P_2O5 (wt%)	Total oxides (wt%)	H_2O (wt%)	CO_2 (ppm)	Li (ppm)	B (ppm)	Rb (ppm)	Sr (ppm)	Y (ppm)	Zr (ppm)	Nb (ppm)	Ba (ppm)	La (ppm)	Nd (ppm)	Hf (ppm)	Th (ppm)	U (ppm)	δ^{11}B	T (°C)	ZrP sat (MPa)
BT01	F6	11-1	77.9	0.10	12.5	0.75	0.06	0.04	0.46	4.60	3.54	0.01	93.5	5.3	103	65	56	169	1.2	17	69	17	2.8	19	12	2.2	15	6.8	3.6	726	164
BT01	F6	11-2	79.7	0.06	12.6	0.71	0.02	0.02	0.50	5.00	1.33	b.d.	90.6	-	-	65	58	153	1.6	19	62	17	2.6	18	13	2.8	14	8.2	1.8	744	-
BT01	F6	12-1	78.3	0.09	12.5	0.73	0.06	0.03	0.52	4.49	3.29	0.01	93.7	4.3	36	68	60	159	0.9	19	70	20	1.1	18	13	3.0	17	8.0	5.8	730	107
Late Bishop Tuff melt inclusion glasses[b]																															
BT02	Ig2NW	1-1	78.4	0.10	11.6	0.72	0.03	0.03	0.40	4.74	3.95	0.01	95.9	-	-	212	42	110	6.4	11	80	12	22	28	14	3.0	14	3.4	3.9	726	-
BT02	Ig2NW	2-1	78.0	0.08	11.9	0.68	0.02	0.04	0.42	4.91	4.01	b.d.	96.0	-	-	209	43	117	6.6	10	72	12	22	17	8.3	2.5	6.5	3.4	3.9	717	-
BT02	Ig2NW	3-1	77.4	0.07	12.3	0.66	b.d.	0.02	0.46	5.00	4.11	0.01	96.5	3.1	286	208	55	142	1.8	12	61	16	2.4	8.8	6.4	2.7	6.7	4.4	3.7	704	102
BT02	Ig2NW	4-1	78.4	0.06	11.8	0.67	0.02	0.04	0.41	4.75	3.79	0.04	96.3	3.3	129	234	48	135	2.5	13	74	15	5.4	16	9.3	3.8	11	5.2	5.7	723	87
BT02	Ig2NW	5-1	78.3	0.09	11.7	0.67	0.05	0.03	0.42	5.00	3.78	b.d.	95.8	2.3	96	209	50	136	2.6	12	80	15	5.2	11	7.1	3.5	8.5	4.6	5.5	726	49
BT02	Ig2NW	6-1	79.2	0.04	11.8	0.61	0.03	0.06	0.40	4.72	3.17	0.02	96.7	-	-	95	55	84	1.9	18	68	16	2.1	16	12	3.6	14	4.8	7.5	726	-
BT02	Ig2NW	6-2	78.3	0.06	12.3	0.73	0.03	0.04	0.45	5.19	2.86	b.d.	97.7	-	-	198	55	136	1.8	14	58	14	2.6	11	6.9	2.7	8.8	4.1	5.5	715	-
BT02	Ig2NW	7-1	78.1	0.06	11.7	0.71	0.02	0.04	0.40	4.94	3.96	0.01	96.4	3.0	b.d.	209	52	144	2.2	13	62	14	4.0	12	8.7	2.7	9.3	4.3	6.5	706	58
BT02	Ig2NW	8-1	78.4	0.04	11.6	0.67	0.03	0.05	0.39	4.90	3.89	b.d.	96.7	3.3	133	218	53	141	2.2	15	109	22	4.6	13	8.4	5.0	11	4.9	3.9	750	88
BT02	Ig2NW	10-1	77.6	0.07	12.2	0.65	0.02	0.06	0.44	4.91	4.10	b.d.	96.7	2.4	68	245	47	128	3.2	12	76	17	8.0	14	7.6	3.1	8.2	4.3	3.9	722	48
Deer Mountain melt inclusion glasses[c]																															
IN02	CP	3-1	76.0	0.05	13.2	1.00	0.02	0.01	0.39	5.14	4.25	b.d.	94.5	3.5	b.d.	161	80	299	17	18	80	24	49	22	13	3.7	13	5.4	3.1	728	69
IN02	CP	4-1	75.1	0.07	13.9	0.77	0.07	0.04	0.40	5.27	4.39	b.d.	94.4	4.9	b.d.	171	92	235	16	18	79	24	48	21	11	3.7	18	7.3	2.5	728	130
IN02	CP	5-1	75.4	0.09	13.6	1.02	0.02	0.01	0.32	5.38	4.12	b.d.	99.0	5.2	b.d.	376	92	216	5.5	21	92	28	20	24	15	4.5	20	5.9	2.8	742	144
IN02	CP	6-1	75.4	0.06	13.7	0.85	−0.02	0.02	0.36	5.25	4.32	b.d.	94.8	4.5	b.d.	-	-	-	-	-	-	-	-	-	-	-	-	-	3.1	-	111
IN02	CP	10-1	74.7	0.06	13.7	0.91	0.09	0.04	1.22	5.19	4.08	0.01	93.9	4.3	b.d.	109	84	204	11	18	84	26	31	17	12	4.4	17	6.9	0.5	725	102
IN02	CP	11-1	74.9	0.04	14.1	0.93	0.02	0.02	0.23	5.40	4.37	b.d.	94.4	3.7	b.d.	129	72	169	22	16	80	26	79	18	12	3.7	16	5.3	2.5	731	77
IN02	CP	12-1	74.7	0.08	14.2	0.89	0.03	0.01	0.36	5.60	4.17	0.02	95.4	5.3	b.d.	-	-	-	-	-	-	-	-	-	-	-	-	-	-	-	149
South Deadman Dome melt inclusion glasses[c]																															
IN01	CP	1-1	78.4	0.07	11.7	0.82	0.04	0.02	0.39	4.65	3.90	0.02	95.2	3.9	b.d.	76	59	155	9.8	15	90	23	49	29	14	4.3	17	5.6	−.3	738	85
IN01	CP	2-1	77.8	0.07	12.4	0.61	0.04	0.05	0.51	4.68	3.82	0.00	94.4	2.6	b.d.	75	58	168	34	13	66	18	124	15	9.4	3.9	15	5.1	2.0	716	40
IN01	CP	3-1	77.7	0.04	12.3	0.70	0.03	0.04	0.56	4.68	3.92	0.00	99.2	3.8	b.d.	99	74	174	24	15	59	19	77	12	10	2.3	14	5.4	0.0	705	81
IN01	CP	7-1	77.5	0.06	12.4	0.73	0.05	0.06	0.55	4.73	3.96	b.d.	99.4	2.6	b.d.	24	39	151	43	17	85	24	112	26	13	2.1	17	6.3	2.6	734	40
IN01	CP	9-1	78.4	0.06	11.9	0.73	0.05	0.02	0.48	4.52	3.85	b.d.	99.8	4.4	b.d.	-	-	-	-	-	-	-	-	-	-	-	-	-	-	-	106
IN01	CP	10-1	78.6	0.05	11.9	0.62	0.03	0.07	0.50	4.56	3.71	b.d.	94.7	4.1	b.d.	68	57	144	40	10	53	13	148	13	8.2	2.3	12	3.9	3.8	700	93
IN01	CP	11-1	78.2	0.07	12.2	0.69	0.03	0.05	0.51	4.56	3.72	0.02	94.4	4.2	b.d.	99	74	161	25	13	62	19	79	15	9.4	2.7	15	5.1	−.5	713	97
IN01	CP	12-1	78.6	0.07	11.8	0.71	0.08	0.04	0.35	4.63	3.67	0.01	99.9	5.1	b.d.	84	75	195	8.1	20	80	22	53	16	13	3.7	17	6.5	0.0	733	139
South Deadman Dome matrix glasses[c]																															
IN01G	FP	1	72.8	0.16	14.8	1.73	0.07	0.11	0.82	5.26	4.23	0.01	100.2	0.27	b.d.	41	27	-	-	-	-	-	-	-	-	-	-	-	5.1	-	-
IN01G	FP	2														44	26	-	-	-	-	-	-	-	-	-	-	-	6.7	-	-
IN01G	FP	3														43	28	157	77	18	234	12	565	38	18	7.7	10	2.9	5.4	-	-
IN01G	FP	4														48	25	170	52	22	254	16	613	63	34	6.2	13	3.8	5.1	-	-
IN01G	FP	5														48	28	185	63	17	303	16	748	49	26	8.6	8.8	3.5	5.7	-	-
IN01G	FP	6														44	28	-	-	-	-	-	-	-	-	-	-	-	5.7	-	-
IN01G	FP	7														43	28	-	-	-	-	-	-	-	-	-	-	-	7.2	-	-
IN01G	FP	8														44	28	-	-	-	-	-	-	-	-	-	-	-	7.5	-	-
IN01G	FP	9														50	26	125	69	23	360	16	748	60	34	8.3	14	3.4	5.6	-	-
IN01G	FP	10														52	30	136	49	19	268	15	612	59	29	7.9	12	3.5	3.8	-	-
IN01G	FP	11														53	27	128	101	20	373	17	962	52	26	8.6	12	3.7	5.6	-	-
Obd01	FP	1	74.0	0.10	13.8	1.61	0.06	0.11	0.88	5.22	4.19	0.01	99.8	0.29	b.d.	43	29	133	19	22	199	16	144	70	33	6.5	18	4.2	4.9	800	-
Obd01	FP	2														-	-	-	-	-	-	-	-	-	-	-	-	-	4.4	-	-
Obd01	FP	3														-	-	-	-	-	-	-	-	-	-	-	-	-	4.7	-	-
Mono Craters[d]																															
Panum Dome	Obsidian	1	77.0	0.05	12.7	0.84	0.04	0.02	0.59	4.66	4.05	0.03	99.9	0.10	b.d.	51	35	142	5.3	21	93	15	23	20	16	3.3	15	4.6	2.6	741	-
Panum Dome	Obsidian	2														-	-	-	-	-	-	-	-	-	-	-	-	-	3.7	-	-
Panum Dome	Obsidian	3														-	-	-	-	-	-	-	-	-	-	-	-	-	3.1	-	-
Upper Dome	Obsidian	1	76.8	0.07	12.7	1.06	0.06	0.03	0.56	4.73	3.99	0.03	100.0	0.24	b.d.	50	34	145	5.8	23	99	18	23	22	18	5.1	19	4.7	2.9	746	-

Table 2 (Contd.)

MC84-df	Obsidian	1	76.8	0.07	12.6	1.08	0.08	0.04	0.53	4.66	4.06	0.01	100.0	0.60	5	48	33	148	5.5	22	87	17	20	20	15	5.2	17	4.3	3.9	736	-
MC84-t	Obsidian	1	76.9	0.06	12.7	1.06	0.06	0.02	0.54	4.65	3.96	0.00	99.7	0.74	5	48	32	149	6.0	21	86	18	20	21	13	4.6	14	5.9	2.9	737	-

[a]Metz and Mahood (1991) stratigraphic units. For major element glasses, average values for three individual analyses are shown. We note good agreement between our data and Metz and Mahood (1991) whole-rock analyses for LV01 and LV03
[b]Stratigraphic units after Wilson and Hildreth (1997). BT01 9-2*hg* Hourglass inclusion
[c]Nomenclature from Sampson (1987). *CP* coarsly porphyritic; *FP* finely porphyritic
[d]Samples from Newman et al. (1988)

Fig. 3 Selected trace elements and H_2O vs. B abundance for Bishop Tuff (**A**–**F**) and post-caldera domes (Deer Mountain and South Deadman Dome) melt inclusion glasses (**G**–**L**). *Error bars* indicated for 1 standard deviation (SD) calculated from replicate measurements of NIST SRM 610. *Stippled fields* in (**A**–**F**) and (**G**–**L**) show range of Bishop Tuff melt inclusions from Anderson et al. (2000) and BT01 and BT02 inclusions (this study), respectively. *Lines* indicate gas-saturated fractional crystallization trends in 20% crystallization steps (see text). $D_{\text{fluid/melt}} = 3$; (Pichavant 1981) and $X_w = 0.04$ (this study). Phase proportions from Sampson and Cameron (1987) and Anderson et al. (2000) were used: Bishop Tuff: quartz (40%), sanidine (43%), plagioclase (15%) and biotite (2%); CP lavas: quartz (8%), sanidine (20%), plagioclase (63%) and biotite (9%); bulk $D_{\text{mineral/melt}}$ values for Bishop Tuff (CP lavas) Sr = 7.1 (7.5), Ba = 12.6 (7.4), Y = 0.06 (0.23), Nb = 0.25 (0.95), Th = 0.02 (0.07) calculated from $D_{\text{mineral/melt}}$ values for rhyolitic melts in Mahood and Hildreth (1983), Ewart and Griffin (1994), and Streck and Grunder (1997)

values that decreased from −69‰ (MC84-df) to −123‰ (Panum Dome).

Seven early Bishop Tuff inclusions with detectable CO_2 (> 5 ppm) define inverse correlation trends between CO_2 and incompatible trace elements (linear correlation coefficients for Y = −0.68; Nb = −0.85; Hf = −0.61;

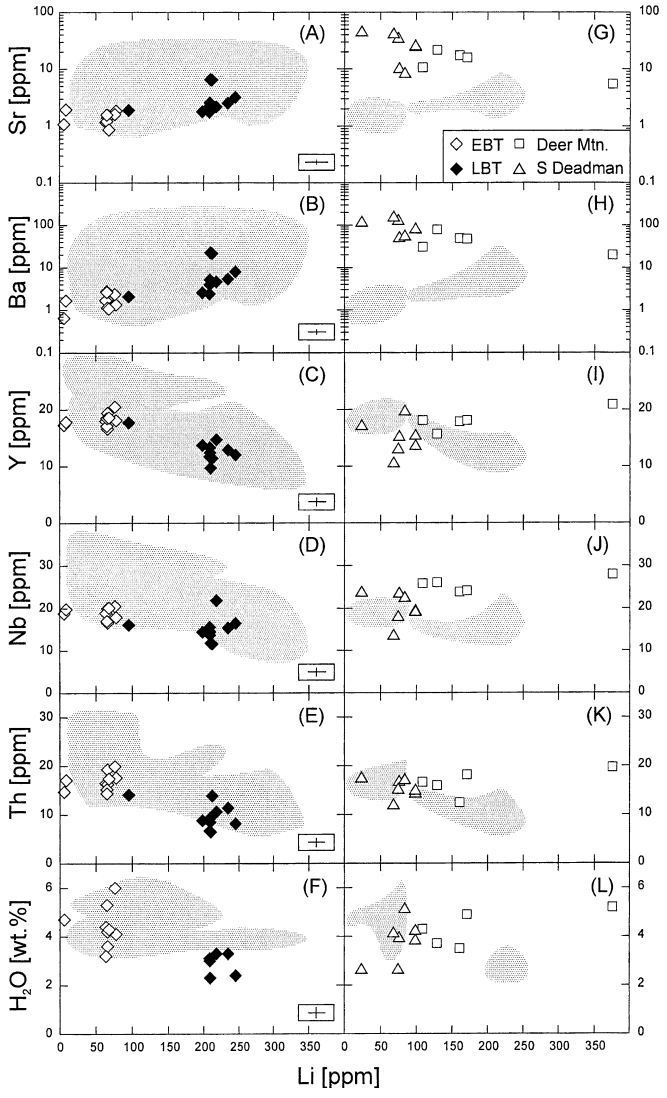

Fig. 4 Selected trace elements and H_2O vs. Li abundance for Bishop Tuff (**A**–**F**) and post-caldera domes (Deer Mountain and South Deadman Dome) melt inclusion glasses (**G**–**L**). See caption of Fig. 3

Th = −0.62). This is consistent with gas-saturated crystallization that was inferred for the early and middle erupted portions of the Bishop rhyolitic magma (Wallace et al. 1995, 1999). Increasing B and H_2O contents from late to early Bishop Tuff (Fig. 3F) are further consistent with isobaric gas-saturated crystallization if the late Bishop melt was richer in CO_2. Melt inclusion data support this assumption (Table 2; Wallace et al. 1999). By contrast, positive correlations between H_2O and incompatible trace elements (including B; Fig. 3L) exist for CO_2-poor Deer Mountain and South Deadman Dome melt inclusions and imply entrapment of gas-undersaturated melts.

If a melt was demonstrably gas-saturated, entrapment pressures can be calculated from dissolved volatile abundances in melt inclusion glasses (e.g., Newman and Lowenstern 2002). For undersaturated melts, pressure-volatile solubility relations allow estimation of minimum pressures. Table 2 summarizes gas-saturation pressures computed for Bishop melt inclusions between ~60 and ~200 MPa (early) and > 50 MPa (late), consistent with previous results (Wallace et al. 1999). From H_2O contents in CP melt inclusions, we infer a similar range of minimum pressures for quartz crystallization (Table 2). This indicates that CP rhyolites crystallized at or below the same depth that was previously occupied by early erupted and presumably shallow portions of the Bishop magma chamber. In this context, we also emphasize that zircon saturation temperatures (Watson and Harrison 1983) calculated for Deer Mountain and South Deadman Dome melt inclusions (average 731 and 720 °C, respectively) are significantly lower than the ~810 °C temperature estimated from Fe-Ti oxide thermometry of CP lavas (Vogel et al. 1989). Similar observations hold for late Bishop Tuff inclusions, but these were originally devitrified and had to be homogenized by laboratory heating. In contrast, pristine melt inclusions from early Bishop Tuff yield zircon saturation temperatures (average 731 °C; Table 2) that agree with Fe-Ti oxide temperatures (~730 °C; Hildreth 1979).

Boron isotope results

Significance of boron isotope variations in Long Valley rhyolites

Individual SIMS boron isotope measurements typically require $\sim 10^6$ times less boron compared to a single conventional TIMS analysis (e.g., Kasemann et al. 2002) and permit analysis of small-volume samples such as melt inclusions. SIMS reproducibility estimated from replicate measurements of NIST SRM 610 during individual analytical sessions (~1.2‰ 1 standard deviation, SD) is less precise than the external reproducibility reported for TIMS boron isotope analysis (~0.5 to 0.8‰; Kasemann et al. 2002). It can be reduced by averaging replicate measurements, provided the materials analyzed are homogeneous. We use the mean square of weighted deviates (MSWD) and trace element data as an estimate for sample homogeneity. For example, 22 individual spot analyses on NIST SRM 610 glass and 10 on BT02 melt inclusion glasses yield weighted averages with MSWD values < 1.5 (well within the 95% confidence boundaries of Mahon 1996), indicating that observed scatter is due to analytical error only. By contrast, seven melt inclusions analyzed from IN01 yield a MSWD > 3 that implies boron isotopic heterogeneity. Trace element compositions corroborate this interpretation: Sr and Ba abundances in melt inclusions vary strongly and correlate with $\delta^{11}B$ (Fig. 5). Figure 5 further illustrates that four low-$\delta^{11}B$ melt inclusions characterized by low Sr and Ba contents are significantly distinct from intermingled high-Sr, high-Ba FP glass of the same lava. Because detectable intra-sample heterogeneity in

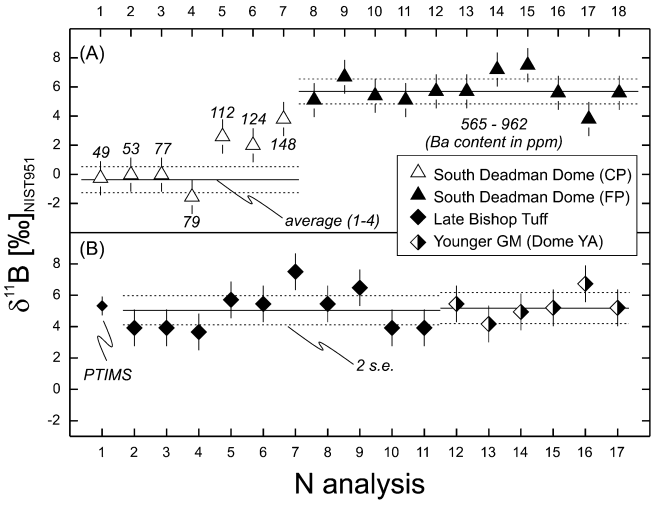

Fig. 5 Results for SIMS boron isotopic measurements of (**A**) South Deadman Dome melt inclusions (IN01) and FP rhyolite glass (IN01G) and (**B**) late Bishop Tuff melt inclusions (BT02) and younger Glass Mountain Dome YA (LV03 and LV04) obsidian. PTIMS analysis of bulk groundmass glass plotted for comparison. *Error bars* 1 standard deviation (SD) computed from replicate measurements of reference materials. *Lines* indicate weighted averages and 95% confidence error envelopes (2 standard errors of mean, *s.e.*). South Deadman Dome CP analyses were ordered according to increasing Ba contents; all others are displayed in analytical sequence. No drift was found over the course of individual analytical sessions. Note that individual analyses of four low-Ba melt inclusions are significantly different from all but one FP rhyolite glass analyses at the 95% confidence level

IN01 is unique in our sample suite, we think that it is permissible to average multiple analyses for other samples. While individual results are listed in Table 2, we will report weighted average $\delta^{11}B$ values (with 2 SE uncertainty stated) in the following.

Comparison between melt inclusions and bulk glass analysis

Figure 3 compares SIMS data of BT02 melt inclusions (late Bishop Tuff) with bulk groundmass glass analyzed by PTIMS. We find excellent agreement between the melt inclusion average ($\delta^{11}B = +5.0 \pm 0.9‰$; 2 SE; MSWD = 1.5; $n = 10$) and the PTIMS result ($+5.4 \pm 0.5‰$; 1 SD). The boron concentration measured for the bulk glass separate (44 ppm) is at the lower end of the melt inclusion range (42–55 ppm).

Late and early Bishop Tuff melt inclusions compared to Glass Mountain obsidians

Early Bishop Tuff melt inclusions yielded a weighted average of $\delta^{11}B = +3.5 \pm 1.0‰$ (MSWD = 1.7; $n = 10$). A single analysis of hourglass inclusion 9-2 yielded indistinguishable $\delta^{11}B = +2.4 \pm 2.3‰$ (not included in weighted average) that is thought to represent groundmass composition. Overall, $\delta^{11}B$ values for early and late Bishop Tuff melt inclusions overlap within error whereas boron concentrations continuously increase from late (42–55 ppm) to early Bishop Tuff (56–64 ppm; Fig. 3), with a maximum of 67 ppm B measured in hourglass inclusion 9-2.

Boron concentrations and isotopic compositions for younger Glass Mountain obsidian that erupted between 0.90 and 0.79 Ma (Metz and Mahood 1985) are indistinguishable from late Bishop Tuff melt inclusions (Fig. 5 and Table 2). This includes two YA Dome glasses sampled at different locations. The older YO Dome (1.06 Ma; Metz and Mahood 1985) yielded the highest $\delta^{11}B$ values measured in this study (average $+7.9 \pm 0.6‰$). For comparison, we also analyzed glasses from older Glass Mountain (1.9–1.3 Ma; Metz and Mahood 1985) and found $\delta^{11}B$ values that range between $+3.4 \pm 0.6‰$ and $+6.4 \pm 0.6‰$ (weighted averages from three to six analyses). While MSWD values close to or < 1 suggest that each sample is homogeneous within the size of the fragments analyzed, three different samples from OC Dome display a subtle $3.0 \pm 2.2‰$ difference in $\delta^{11}B$. Because OC obsidians are also inhomogeneous in their trace element composition (Table 2), we suspect that boron isotopic variations are due to magma heterogeneities and are unrelated to secondary effects such as weathering.

Deer Mountain, Inyo and Mono Lavas

Boron concentrations in Deer Mountain melt inclusions are high (~90 ppm) and their average boron isotopic composition ($+2.2 \pm 0.8‰$; MSWD = 1.1; $n = 6$) is lower than the average values for Bishop Tuff and younger Glass Mountain rhyolite. Quartz crystals from South Deadman Dome CP lava (IN01) host inclusions with highly variable trace element and boron abundances (between 35 and 75 ppm). As pointed out in 4.2.1, the boron isotopic composition of the four most evolved inclusions (average $-0.4 \pm 1.0‰$; MSWD = 0.3) is significantly lower than that of FP rhyolite glass IN01G (average $+5.7 \pm 0.8‰$; MSWD = 0.4; $n = 11$). Three analyses of FP rhyolite from the nearby Obsidian Dome yielded a $\delta^{11}B$ weighted average of $+4.7 \pm 1.0‰$ (MSWD = 0.1) that overlaps within uncertainties with FP South Deadman Dome rhyolite. Boron contents in all FP glasses are similar (28 ± 1 ppm), but much lower than those measured in Bishop Tuff and Glass Mountain samples (Table 2).

Four samples of coeval Mono Craters rhyolites have slightly higher boron contents (33 ± 1 ppm) and somewhat lower $\delta^{11}B$ values (average $+3.2 \pm 0.8‰$, MSWD = 0.4) than sample IN01G (Fig. 6). The boron isotopic homogeneity of Mono Craters rhyolites is remarkable given the fact that open-system degassing significantly changed their hydrogen isotopic composition (Newman et al. 1988). Despite a ~50‰ decrease in δD over an eight-fold depletion in dissolved H_2O, boron concentrations and isotopic compositions are invariant within error.

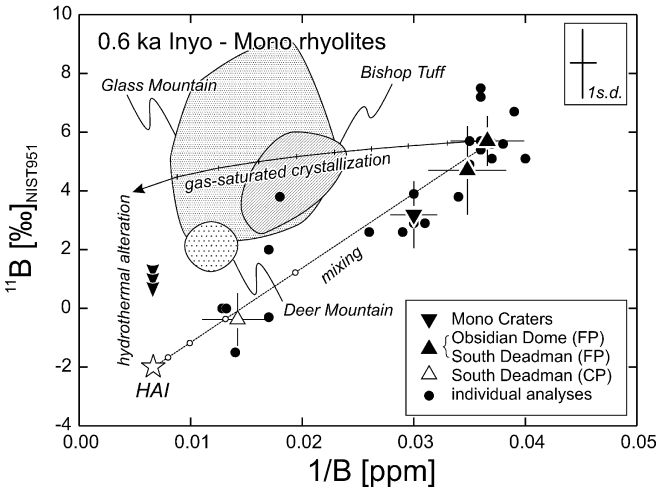

Fig. 6 Average boron isotopic composition vs. 1/B for 0.6 ka Inyo-Mono rhyolites (*2 s.e. error bars*). Individual analyses (*1 SD error bars*) and fields for average compositions of other sample groups (pre-caldera Glass Mountain obsidian, Bishop Tuff and Deer Mountain) plotted for comparison. Gas-saturated crystallization trend (*tick marks* for 10% steps in mass of remaining melt) was calculated for $X_w = 0.04$ and T = 750 °C (see text). $D_{fluid/melt} = 3$ and $\alpha_{silicate/fluid} = 0.994$ from Pichavant (1981) and Hervig et al. (2002), respectively. *Open star* indicates model composition of hydrothermally altered intrusions (HAI). Although the HAI component is modeled as a point (120 ppm B similar to the highest values measured in pre-caldera rhyolites and $\delta^{11}B = -2‰$; this is a ~5‰ shift from the lowest 'magmatic' values measured in pre-caldera rhyolites equivalent to the ^{11}B depletion in hydrothermally altered rhyolites from Yellowstone; Palmer and Sturchio 1990), it is recognized that it may exhibit compositional heterogeneity. First-order mixing calculations indicate ~40% HAI component in South Deadman Dome CP rhyolite

Discussion

Eruptive degassing: no detectable effect on boron isotopes

Shielding of melt inclusions by surrounding host quartz plausibly minimizes boron loss that potentially affects groundmass glasses due to interaction with hydrothermal fluids (Shaw and Sturchio 1992) or devitrification (Higgins 1988). As pointed out by Wallace et al. (1999) and Anderson et al. (2000), melt inclusions from Bishop Tuff largely preserved their initial dissolved volatiles and reliably record variations in melt composition over the period of inclusion entrapment. Indistinguishable $\delta^{11}B$ values for BT02 groundmass glass and melt inclusions (Fig. 3) thus imply insignificant isotopic fractionation due to eruptive degassing or post-depositional alteration. Comparatively low boron contents in BT02 groundmass glass could indicate minor boron loss, but alternative explanations are equally plausible: while closed-system crystallization produces enriched residual melts compared to earlier trapped melt inclusions, inverse compositional trends might indicate that crystals originated from a different source. In fact, the evolved composition of hourglass inclusion BT01 9-2 is consistent with closed-system crystallization of the early Bishop Tuff, whereas inverse zoning of melt inclusions in phenocrysts and comparatively less evolved groundmass glass compositions in the late Bishop Tuff imply that crystals became ultimately entrained in a more primitive magma (Dunbar and Hervig 1992; Wallace et al. 1999; Anderson et al. 2000).

The lack of significant boron loss and isotopic fractionation during eruptive degassing is underlined by the homogeneity of four Mono Craters obsidian glasses (Table 2) despite well-documented variations in H_2O content and δD values (Newman et al 1988). We further measured indistinguishable boron isotopic compositions in BT02 melt inclusion glasses and younger Glass Mountain obsidians (LV03 and LV04; Fig. 3) that are in line with radiogenic and oxygen isotopic evidence that indicate compositional similarity between Bishop Tuff and younger Glass Mountain (Halliday et al. 1984, 1989; Bindeman and Valley 2002). In summary, we find that compositionally related rhyolitic glasses have indistinguishable boron contents despite strong variations in dissolved volatiles and conclude that the pre-eruptive boron isotopic signature remained largely unchanged by the eruption process.

Secondary boiling and degassing—boron variations in comparison with experimental results

Gas-saturated conditions were inferred for the Bishop magma (see Wallace et al. 1995, 1999). We now aim to test how secondary boiling (volatile exsolution due to cooling and crystallization) prior to eruptive degassing affected boron and other components in the melt by using experimental data on boron partitioning between rhyolitic melt and hydrous gas phase (Hervig et al. 2002). We adopt the approach by Candela (1986) and model boron variations by mass balance between anhydrous crystals (no boron uptake), hydrous melt, and vapor phase:

$$c_l = c_o f^{\left(D_{fluid/melt} \cdot X_w\right) - 1}$$

(C_l and C_o = concentration of boron in remaining iquid and original liquid, respectively, after onset of water saturation; f = fraction of remaining melt, $D_{fluid/melt}$ = partition coefficient between vapor and melt; X_w = weight fraction of H_2O in melt). Model results for boron and selected trace elements are displayed in Fig. 3 (A–E). To a first approximation, gas-saturated fractionation curves are consistent with observed variations in Bishop melt inclusions. Note that apparent deviations could result from uncertainties in mineral-melt D values or starting compositions, but at least for the more incompatible elements (Fig. 3C–E) gas-undersaturated crystallization would further enhance these deviations.

While similar trends as for B should be expected for Li (with $D_{fluid/melt} > 1$ at pressures < 400 MPa; Webster et al. 1989), the bimodal distribution of Li abundance in

early and late inclusions (Fig. 4) appears inconsistent with a continuous differentiation trend. The interpretation of Fig. 4 is further complicated by extremely low Li abundances, e.g. in one hourglass inclusion (~9 ppm; consistent with findings by Wallace et al. 1999). This leads us to suspect that Li is potentially more strongly affected by leaking, eruptive degassing or post-depositional alteration than B, although invariant Li contents equivalent to early Bishop Tuff are preserved in younger Glass Mountain obsidian (Table 2). In conclusion, we think that gas-saturated crystallization reasonably well explains trace element vs. B trends in Bishop Tuff melt inclusions, but some aspects regarding the origin of compositional variations including Li remain unresolved (cf. Anderson et al. 2000).

For gas-saturated crystallization, melt depletion in ^{11}B is predicted from experimental isotopic fractionation factors ($\alpha_{melt/fluid}$) that range between 0.993 and 0.994 (Hervig et al. 2002) at relevant temperatures (T = 700–800 °C). A potential isotopic fractionation between melt and biotite can be reasonably neglected because boron uptake by minor quantities of biotite is insignificant (Tonarini et al. 2003). Rayleigh fractionation is reasonably assumed because boron in the gas phase will be rapidly removed due to the density contrast between silicate melt and aqueous fluid. We accordingly calculated minor depletion in ^{11}B (−0.5‰) that agrees with the apparent isotopic homogeneity of melt inclusion glasses from early and late Bishop Tuff (−1.5 ± 1.9‰ difference in average $\delta^{11}B$ and ~20% increase from ~50 ppm B in late Bishop Tuff). It also follows that experimental data for boron partitioning are concordant with observed boron behavior in metaluminous systems despite the fact that experiments were calibrated for peraluminous compositions (Hervig et al. 2002).

For post-caldera dome inclusions, the modeled gas-saturated fractionation trends clearly fail to match measured variations, in particular for compatible trace elements such as Sr and Ba (Fig. 3G, H). Furthermore, a $\delta^{11}B$ shift of −1.2‰ is predicted for ~65% gas-saturated crystallization of South Deadman Dome FP rhyolite (i.e., from ~25 to ~75 ppm B; upper curve in Fig. 6). This compares unfavorably with the observed −6.1 ± 1.8‰ difference between IN01G and IN01 glasses. Alternatively, we thus suggest open-system mixing and/or assimilation to explain the overall ~8‰ variations in $\delta^{11}B$ measured in Long Valley glasses.

Alternative scenario: assimilation of low-temperature altered intrusions

Constraints for end-members and mixing processes

Open-system processes have been previously invoked for Long Valley based on a variety of observations: magma mingling (e.g., Sampson and Cameron 1987; Varga et al. 1990), compositional and isotopic variations (e.g., Vogel et al. 1989; Halliday et al. 1989; Metz and Mahood 1991; Knesel and Davidson 1997; Heumann and Davies 1997), isotopic heterogeneity of phenocrysts (e.g., Davies and Halliday 1998); reverse mineral or melt inclusion zonation patterns (e.g., Dunbar and Hervig 1992; Anderson et al. 2000). Consequently, we interpret boron isotopic variations in post-caldera rhyolites to result from some form of mixing process. In order to better characterize potential end-members and the nature of this process, we discuss additional evidence, in particular from trace elements and Nd isotopes. Our main observations can be summarized as follows:

1. Boron abundances in melt inclusion glasses correlate with fluid immobile elements (e.g., Y, Nb, Th; Sturchio et al. 1986; Fig. 3). This strongly argues against boron addition via a fluid phase. On the other hand, evolved silicic melts can be highly enriched in both B and Nb (e.g., Leeman and Sisson 1996) and this is observed in Older Glass Mountain rhyolites;
2. From the extrapolated trends in the Sr vs. B diagram (Fig. 3G), we infer low Sr abundances for the high-B end-member. Assimilation-fractional crystallization models further illustrate why assimilation of typical Sierran wall-rocks is unlikely because it would result in hybrid melts that have higher Sr than measured in CP melt inclusions (upper curve in Fig. 7A). In contrast, assimilation of low-Sr and high-B rocks would satisfy mass balance constraints (lower curve in Fig. 7A);
3. Despite a more than three-fold increase of boron concentrations in post-caldera rhoylite glasses, whole-rock ϵNd values for FP and CP lavas overlap (Fig. 7B). This is consistent with FP rhyolite assimilating a boron-rich end-member similar in ϵNd, rather than Sierran crust with typically much lower ϵNd (upper and lower curve in Fig. 7B, respectively). Note that we did not attempt to correlate our glass data with published $^{87}Sr/^{86}Sr$ analyses because whole-rock Sr data are controlled by plagioclase and, consequently, potentially biased by the presence of xenocrysts (cf. Davies and Halliday 1998);
4. While the boron isotopic composition of potential source reservoirs remains elusive, we would expect some correlation between $\delta^{11}B$ and ϵNd, if boron isotopic signatures were inherited from a mantle-derived parental magma that experienced variable degrees of crustal contamination. This is not observed, however. For example, $\delta^{11}B$ values for older Glass Mountain and Inyo FP lava overlap, whereas their Nd-isotopic compositions are clearly distinct (Figs. 6 and 7);
5. Assimilation of preexisting intrusive rocks by fresh rhyolite recharge seems geologically and petrologically plausible: the two most ^{11}B depleted rhyolites are post-caldera domes and located inside the caldera margins (Fig. 1). In particular, South Deadman Dome exhibits evidence for magma mingling, thermal rejuvenation (i.e., zircon saturation temperatures fall well below the eruption temperature)

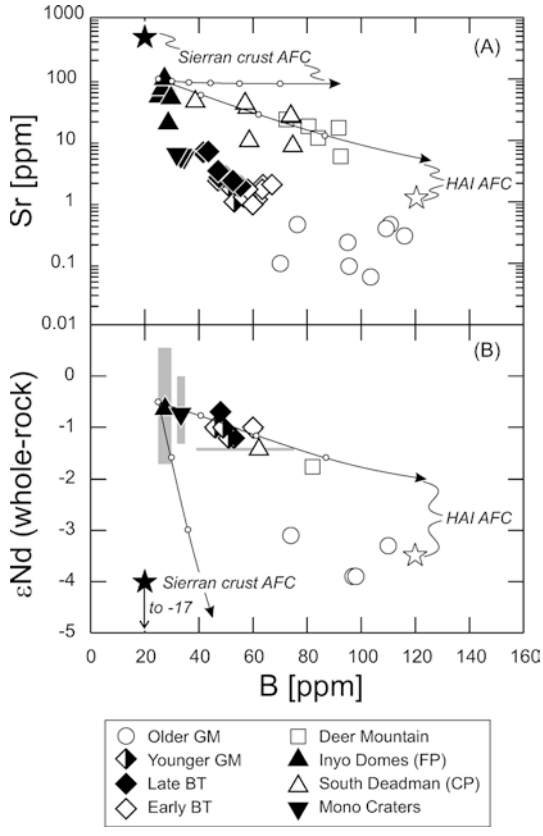

Fig. 7 Sr vs. B (**A**) and Nd-isotopic composition of whole-rocks vs. B for Long Valley glasses (**B**). Average values for ϵNd plotted as *symbols*; range is indicated by *solid bars*. Data sources: Sampson and Cameron (1987); Palacz and Gill (1994); Heumann and Davies (1997); Davies and Halliday (1998). Assimilation-fractional crystallization (AFC) trends were calculated for primitive rhyolite and Sierran wall-rocks (*solid star* with Sr = 500 ppm: Hildreth 1979; Nd = 26 ppm: average upper crust in Taylor and McLennan 1995; 20 ppm B: average upper crust in Leeman and Sisson 1996; ϵNd = −11: average from values compiled in Halliday et al. 1984) and HAI (*open star* with Sr = 1 ppm; Nd = 18 ppm; B = 120 ppm: equivalent to older Glass Mountain rhyolite in Table 2). Sr bulk D = 3.5 (Nd = 2.2) calculated from mineral proportions in FP lava (Sampson and Cameron 1987) and $D_{\text{mineral/melt}}$ values for rhyolites (Mahood and Hildreth 1983; Nash and Crecraft 1985; Ewart and Griffin 1994). Presence of 0.1% allanite, incompatible behavior of boron and a ratio for assimilation/crystallization rates of 0.5 was assumed; *tick marks* for 10% steps in mass of remaining melt

and zircon crystals that significantly predate the eruption (Reid et al. 1997).

In synthesizing our observations, we rule out a significant role of regional country rocks for the origin of ^{11}B depletion in CP post-caldera rhyolites and instead favor assimilation of hydrothermally altered intrusive margins by recharge of more primitive rhyolitic magma. For this to happen, we expect that low temperature fluid-rock exchange shifted "magmatic" δ^{11}B values of compositional equivalents to Glass Mountain rhyolites (δ^{11}B $\sim +3$–$+8$‰; Fig. 6) to isotopically lighter values (e.g., Palmer and Sturchio 1990; Hervig et al. 2002).

^{11}B depleted rhyolites: an equivalent to low-δ^{18}O magmas?

Assimilation of hydrothermally altered materials has been previously invoked for the generation of low-δ^{18}O magmas (e.g., Mt. Mazama: Bacon et al. 1989; Yellowstone: Bindeman and Valley 2000, 2001). Our limited boron isotope data set provides some indication that similar processes should not be ruled out for Long Valley, in particular for post-caldera rhyolites, despite the fact that so far they have gone undetected by oxygen isotopes (Bindeman and Valley 2002). Oxygen isotope data for hydrothermally altered rocks from Long Valley show considerable deviations from magmatic values (e.g., Smith and Suemnicht 1991; McConnell et al. 1997; Mukhopadhyay 2002). Because these samples were either from the surface or from drill holes that only penetrated caldera-fill and shallow Mesozoic roof rocks, we think they are not representative for the deeper-seated intrusive complex. Volatile saturation pressure estimates for the least degassed Deer Mountain and South Deadman Dome melt inclusions (Table 2) indeed imply that ^{11}B depleted melts became entrapped at >140 MPa, equivalent to >6 km depth assuming a 2.5-g/cm^3 density of felsic cap rocks. Because intrusive rock samples from such depths are unavailable for direct comparison, we summarize theoretical constraints to speculate why assimilation of chilled intrusive margins potentially remained subtle or undetectable by oxygen isotope analysis:

1. low-δ^{18}O meteoric waters might be diluted or absent in deep-circulating fluids released from cooling volatile-rich magmas;
2. during hydrothermal alteration involving dominantly orthomagmatic fluids (initial δ_{fluid} = initial δ_{rock}), the isotopic shifts in δ^{11}B and δ^{18}O depend on their respective equilibrium fractionation factors, which at 300 °C are about ~15 times larger for boron than for oxygen (notice the opposite sense of fractionation: ^{11}B is enriched in the fluid whereas ^{18}O is depleted; Williams et al. 2001);
3. at a given water/rock ratio, the isotopic shifts scale with concentration ratios for the exchanged element between fluid and rock (Criss and Taylor 1986). For oxygen, this ratio is fixed to 1.8 (Criss and Taylor 1986), whereas boron-metasomatism via hydrothermal fluids is common (Leeman and Sisson 1996). Partial melting of such rocks would further enrich boron in the melt due to its incompatibility in most silicates. Thus the hydrothermally altered end-member can have more leverage on boron in hybrid rocks compared to oxygen with equal abundance in silicic rocks and melts.

Implications for magma sources

Boron isotopic compositions (δ^{11}B between +0 to +8‰) measured in selected Long Valley rhyolites are

the highest values so far reported for Quaternary-Holocene rocks in the Western USA: unaltered hot-spot rhyolites (Yellowstone: −5‰; Palmer and Sturchio 1990) and subduction-related andesites (Mt. Shasta olivine-hosted melt inclusions: −21 to 0‰; Rose et al. 2001) have considerably lighter boron isotopic compositions. It has been argued that a major component in Long Valley silicic magmas was mantle derived and their parental magmas became crustally contaminated (e.g., Halliday et al. 1984, 1989). Unfortunately, little is known about boron in potential crustal contaminants such as the Sierran batholiths (Hildreth 1979). Comparatively low $\delta^{11}B$ values typical for tourmaline as the dominant host for boron in crustal rocks (between ~0 and −20‰; Palmer and Swihart 1996; Kasemann et al. 2001), however, imply that crustal contamination is unlikely to result in strongly positive $\delta^{11}B$ values. Depleted mantle ($\delta^{11}B = -7$; Chaussidon and Jambon 1994) can further be ruled out as the primary source of boron. Alternatively, positive $\delta^{11}B$ signatures and high boron concentrations could result from melting of sea-water altered oceanic crust (e.g., serpentinites with $\delta^{11}B$ of +7–+13‰; Spivack and Edmond 1987) or mantle to which boron-rich fluids derived from dehydration of subducted oceanic crust has been added (Rose et al. 2001). We thus speculate that the deep-seated roots of the Long Valley magma system became infiltrated by boron-rich fluids of heavy isotopic composition at some point in their geologic past, presumably during Cenozoic subduction. Boron isotopic studies of coeval Long Valley mafic rocks (e.g., Cousens 1996) are needed to further test this hypothesis.

Conclusions

1. Indistinguishable $\delta^{11}B$ values in variably degassed glasses (i.e., melt inclusions with $H_2O = \sim 3$ to 6 wt% and degassed matrix glasses with $H_2O < 0.8$ wt%) indicate that eruptive degassing and post-depositional alteration had no detectable effects on boron isotopic compositions of fresh pumice and obsidian erupted from Long Valley.
2. Published partitioning and fractionation coefficients for boron predict significant isotopic fractionation during pre-eruptive degassing (secondary boiling) only for magmas that have undergone extensive fractional crystallization under gas-saturated conditions (i.e., ~2‰ for 90% isobaric crystallization of a rhyolitic melt at $X_w = 0.04$ and 750 °C). Rhyolite glasses from Long Valley, however, show a much stronger decrease in $\delta^{11}B$ over comparatively small increases in boron and incompatible trace elements abundances. Isotopic fractionation between melt and vapor at magmatic temperatures is therefore unlikely to have produced melts significantly depleted in ^{11}B.
3. Low-temperature alteration involving orthomagmatic fluids has the potential to deplete ^{11}B in rocks. This is based on empirical and experimental evidence for strong isotopic fractionation during subsolidus exchange of boron between silicates and fluid (e.g., Palmer and Sturchio 1990; Hervig et al. 2002). Comparatively low $\delta^{11}B$ values were measured in melt inclusion glasses from post-caldera lavas. These also indicate near-solidus inclusion trapping temperatures as low as ~700 °C, reheating to ~810 °C (Vogel et al. 1989), and entrapment pressures that are equivalent to the depths at which rhyolitic magmas partially crystallized during the caldera-forming stage. In the light of these observations, we favor assimilation of ^{11}B depleted, hydrothermally altered sub-caldera intrusive rocks triggered by recharge of fresh rhyolite.
4. Similar mechanisms have been invoked for the origin of low-$\delta^{18}O$ rhyolites erupted from other silicic magma systems (e.g., Bacon et al. 1989). We propose that boron isotopes provide a complementary tracer for hydrothermal alteration and assimilation of otherwise compositionally indistinguishable chilled margin rocks, in particular if deep-reaching meteoric waters were absent. By the same token, we urge caution in the use of boron isotopes as source indicators in long-lived composite magma systems.
5. "Defrosting" of the crystallized rind of the Bishop Tuff magma chamber just prior to eruption has been previously proposed (Mahood 1990). Thermal rejuvenation by input of fresh magma followed by partial remobilization of intrusive rocks plausibly causes recycling of earlier formed crystals. This might explain some of the apparent long crystal residence times (e.g., Mahood 1990; van den Bogaard and Schirnick 1995; Christensen and Halliday 1996; Reid et al. 1997; Davies and Halliday 1998) that are in conflict with thermal constraints requiring rapid heat-dissipation from shallow magma bodies (Sparks et al. 1990).

Acknowledgements Several samples included in this study were kindly provided by M.R. Reid (late Bishop Tuff and Glass Mountain) and S. Newman (Mono Craters). R. Kessel and A. Nienhaus are thanked for field assistance, and hospitality by J. C. Harvey is gratefully acknowledged. We also thank the members of the UCLA ion probe group, T. M. Harrison, M. Grove, G. Jarzebinski and K. McKeegan. Discussions with J. Vazquez helped to inspire some of the ideas presented here. J. Erzinger, W. Heinrich, M. Koch-Müller and D. Rhede (GeoForschungsZentrum Potsdam) and Andrew Berry and Nick Ware (Australian National University) are thanked for providing access to infrared spectrometry and electron microprobe facilities. A. Meixner kindly contributed the PTIMS analysis. Funding was provided by a DOE grant to UCLA (4-443875-MH-22 400) and NSF grant (EAR0003601) that supports JIS. The UCLA ion microprobe is partially supported by a grant from the NSF Instrumentation and Facilities Program. An informal review by K. McKeegan and journal reviewers G. Davies, M. Chaussidon as well as an anonymous reviewer helped to clarify this presentation.

References

Anderson AT, Davis AM, Lu F (2000) Evolution of Bishop Tuff rhyolitic magma based on melt and magnetite inclusions and zoned phenocrysts. J Petrol 41:449–473

Bacon CR, Adami LH, Lanphere MA (1989) Direct evidence for the origin of low- $\delta^{18}O$ silicic magmas; quenched samples of a magma chamber's partially-fused granitoid walls, Crater Lake, Oregon. Earth Planet Sci Lett 96:199–208

Bailey RA, Dalrymple GB, Lanphere MA (1976) Volcanism, structure, and geochronology of Long Valley caldera, Mono Country, California. J Geophys Res B 81:725–744

Bailey RA (1989) Geologic map of the Long Valley caldera, Mono-Inyo-Craters volcanic chain, and vicinity, eastern California. US Geol Surv Misc Invest Series Map I-1933I-1933 (1:62500)

Bindeman IN, Valley JW (2000) Formation of low- $\delta^{18}O$ rhyolites after caldera collapse at Yellowstone, Wyoming, USA. Geology 28:719–722

Bindeman IN, Valley JW (2001) Low-$\delta^{18}O$ rhyolites from Yellowstone; magmatic evolution based on analyses of zircons and individual phenocrysts. J Petrol 42:1491–1517

Bindeman IN, Valley JW (2002) Oxygen isotope study of the Long Valley magma system, California: isotope thermometry and convection in large silicic magma bodies. Contrib Mineral Petrol 144:185–205

Candela PA (1986) Toward a thermodynamic model for the halogens in magmatic systems: an application to melt-vapor-apatite equilibria. Chem Geol 57:289–301

Chaussidon M, Jambon A (1994) Boron content and isotopic composition of oceanic basalts; geochemical and cosmochemical implications. Earth Planet Sci Lett 121:277–291

Chaussidon M, Robert F, Mangin D, Hanon P, Rose EF (1997) Analytical procedures for the measurement of boron isotope composition by ion microprobe in meteorites and mantle rocks. Geostandard Newsl 21:7–17

Christensen JN, DePaolo DJ (1993) Time scales of large volume silicic magma systems; Sr isotopic systematics of phenocrysts and glass from the Bishop Tuff, Long Valley, California. Contrib Mineral Petrol 113:100–114

Christensen JN, Halliday AN (1996) Rb-Sr ages and Nd isotopic compositions of melt inclusions from the Bishop Tuff and the generation of silicic magma. Earth Planet Sci Lett 144:547–561

Cousens BL (1996) Magmatic evolution of Quaternary mafic magmas at Long Valley Caldera and the Devils Postpile, California; effects of crustal contamination on lithospheric mantle-derived magmas. J Geophys Res B 101:27673–27689

Criss RE, Taylor HP Jr (1986) Meteoric-hydrothermal systems. In: Valley JW, Taylor HP Jr, O'Neil JR (eds) Stable isotopes in high temperature geological processes. Rev Mineral 16:373–424

Davies GR, Halliday AN, Mahood GA, Hall CM (1994) Isotopic constraints on the production rates, crystallisation histories and residence times of precaldera silicic magmas, Long Valley, California. Earth Planet Sci Lett 125:17–37

Davies GR, Halliday AN (1998) Development of the Long Valley rhyolitic magma system; strontium and neodymium isotope evidence from glasses and individual phenocrysts. Geochim Cosmochim Acta 62:3561–3574

Dunbar NW, Hervig RL (1992) Petrogenesis and volatile stratigraphy of the Bishop Tuff; evidence from melt inclusion analysis. J Geophys Res B 97:15129–15150

Ewart A, Griffin WL (1994) Application of proton-microprobe data to trace-element partitioning in volcanic rocks. Chem Geol 117:251–284

Ewert JW, Harpel CJ (2000) Bibliography of literature pertaining to Long Valley Caldera and associated volcanic fields. US Geol Survey Open-File Rep 00–221:1–156

Halliday AN, Fallick AE, Hutchinson J, Hildreth W (1984) A Nd, Sr and O isotopic investigation into the causes of chemical and isotopic zonation in the Bishop Tuff, California. Earth Planet Sci Lett 68:379–391

Halliday AN, Mahood GA, Holden P, Metz JM, Dempster TJ, Davidson JP (1989) Evidence for long residence times of rhyolitic magma in the Long Valley magmatic system; the isotopic record in precaldera lavas of Glass Mountain. Earth Planet Sci Lett 94:274–290

Hervig RL, Moore GM, Williams LB, Peacock SM, Holloway JR, Roggensack K (2002) Isotopic and elemental partitioning of boron between hydrous fluid and silicate melt. Am Mineral 87:769–774

Heumann A, Davies GR (1997) Isotopic and chemical evolution of the post-caldera rhyolitic system at Long Valley, California. J Petrol 38:1661–1678

Heumann A, Davies GR, Elliott T (2002) Crystallization history of rhyolites at Long Valley, California, inferred from combined U-series and Rb-Sr isotope systematics. Geochim Cosmochim Acta 66:1821–1837

Higgins MD (1988) Trace element geochemistry of the Inyo volcanic chain, California; evidence for multiple magma sources, magma mixing and post-eruption loss of boron. J Volcanol Geotherm Res 35:97–110

Hildreth W (1979) The Bishop Tuff: evidence for the origin of compositional zonation in silicic magma chambers. In: Chapin CE, Elston WE (eds) Ash-flow tuffs. Geol Soc Am Spec Pap 180:43–75

Hildreth W (1981) Gradients in silicic magma chambers: implications for lithospheric magmatism. J Geophys Res B 86:10153–10192

Ishikawa T, Nakamura E (1994) Origin of the slab component in arc lavas from across-arc variation of B and Pb isotopes. Nature 370:205–208

Kasemann S, Erzinger J, Franz G (2001) Boron recycling in the continental crust of the central Andes from the Palaeozoic to Mesozoic, NW Argentina. Contrib Mineral Petrol 140:328–343

Kasemann S, Meixner A, Rocholl A, Vennemann T, Schmitt A, Wiedenbeck M (2002) Boron and oxygen isotope composition of microanalytical reference materials NIST SRMs 610/612, JB-2G and JR-2G. Geostandard Newsl 25:405–416

Kelleher PC, Cameron KL (1990) The geochemistry of the Mono Craters-Mono Lake Islands Volcanic Complex, eastern California. J Geophys Res B 95:17643–17659

Knesel KM, Davidson JP (1997) The origin and evolution of large-volume silicic magma systems; Long Valley Caldera. Int Geol Rev 39:1033–1052

Leeman WP, Sisson VB (1996) Geochemistry of boron and its implications for crustal and mantle processes. In: Grew ES, Anovitz LM (eds) Boron: mineralogy, petrology and geochemistry. Rev Mineral 33:645–707

Lindsay JM, Schmitt AK, Trumbull RB, de Silva SL, Siebel W, Emmermann R (2001) Magmatic evolution of the La Pacana Caldera system, central Andes, Chile: compositional variation of two cogenetic, large-volume felsic ignimbrites and implications for contrasting eruption mechanisms. J Petrol 42:459–486

Mahon K (1996) The New 'York' regression: application of an improved statistical method to geochemistry. Int Geol Rev 38:293–303

Mahood GA (1990) Second reply to comment of Sparks RSJ, Huppert HE, Wilson CJN on ''Evidence for long residence times of rhyolitic magma in the Long Valley magmatic system: the isotopic record in the precaldera lavas of Glass Mountain''. Earth Planet Sci Lett 99:395–399

Mahood GA, Hildreth EW (1983) Large partition coefficients for trace elements in high-silica rhyolites. Geochim Cosmochim Acta 47:11–30

McConnell VS, Valley JW, Eichelberger JC (1997) Oxygen isotope compositions of intracaldera rocks; hydrothermal history of the Long Valley Caldera, California. J Volcanol Geotherm Res 76:83–109

Metz JM, Bailey RA (1993) Geologic map of Glass Mountain, Mono Country, California. US Geol Surv Map I-1995

Metz JM, Mahood GA (1984) Eruptive history of Glass Mountain, Long Valley, California: precursors to a large explosive eruption. US Geol Surv Rep Open-File Rep 84-0939:41–75

Metz JM, Mahood GA (1985) Precursors to the Bishop Tuff eruption: Glass Mountain, Long Valley, California. J Geophys Res B 90:11121–11126

Metz JM, Mahood GA (1991) Development of the Long Valley, California, magma chamber recorded in precaldera rhyolite lavas of Glass Mountain. Contrib Mineral Petrol 106:379–397

Miller CD (1985) Holocene eruptions at the Inyo volcanic chain, California: Implications for possible eruptions in Long Valley caldera. Geology 13:14–17

Mukhopadhyay B (2002) Water-rock interactions in the basement beneath Long Valley Caldera; an oxygen isotope study of the Long Valley Exploratory Well drill cores. J Volcanol Geotherm Res 116:325–359

Nash WP, Crecraft HR (1985) Partition coefficients for trace elements in silicic magmas. Geochim Cosmochim Acta 49:2309–2322

Newman S, Epstein S, Stolper E (1988) Water, carbon dioxide, and hydrogen isotopes in glasses from the ca. 1340 A.D. eruption of the Mono Craters, California; constraints on degassing phenomena and initial volatile content. J Volcanol Geotherm Res 35:75–96

Newman S, Lowenstern JB (2002) VolatileCalc: a silicate melt-H_2O-CO_2 solution model written in Visual Basic for Excel. Comp Geosci 28:597–604

Palacz Z, Gill J (1994) Pb, Sr, Nd isotope and U-series investigation of the Holocene Inyo and Mono high silica rhyolite domes, E. California. In: Lanphere MA, Dalrymple GB, Turrin BD (eds) Abstracts of the Eighth International Conference on Geochronology, Cosmochronology, and Isotope Geology. US Geol Surv Circ, 241 pp

Palmer MR (1991) Boron-isotope systematics of Halmahera Arc (Indonesia) lavas; evidence for involvement of the subducted slab. Geology 19:215–217

Palmer MR, Sturchio NC (1990) The boron isotope systematics of the Yellowstone National Park (Wyoming) hydrothermal system; a reconnaissance. Geochim Cosmochim Acta 54:2811–2815

Palmer MR, Swihart GH (1996) Boron isotope geochemistry: an overview. Geochemistry of boron and its implications for crustal and mantle processes. In: Grew ES, Anovitz LM (eds) Boron: mineralogy, petrology and geochemistry. Rev Mineral 33:709–744

Pearce NJG, Perkins WT, Westgate JA, Gorton MP, Jackson SE, Neal CR, Chenery SP (1995) A compilation of new and published major and trace element data for NIST SRM 610 and NIST SRM 612 glass reference materials. Geostandard Newsl 21:115–144

Pichavant M (1981) An experimental study of the effect of boron on a water saturated haplogranite at 1 kb vapor pressure. Contrib Mineral Petrol 76:430–439

Reid MR, Coath CD, Harrison TM, McKeegan KD (1997) Prolonged residence times for the youngest rhyolites associated with Long Valley Caldera; ^{230}Th-^{238}U ion microprobe dating of young zircons. Earth Planet Sci Lett 150:27–39

Reid MR, Coath CD (2000) In situ U-Pb ages of zircons from the Bishop Tuff; no evidence for long crystal residence times. Geology 28:443–446

Rinehart CD, Ross DC (1957) Geology and mineral deposits of the Mount Morrison quadrangle, Sierra Nevada, California, with a section on a gravity study of Long Valley by Pakiser LC. US Geol Surv Prof Pap 385:1–104

Rose EF, Shimizu N, Layne GD, Grove TL (2001) Melt production beneath Mt. Shasta from boron data in primitive melt inclusions. Science 293:281–283

Sarna Wojcicki AM, Pringle MS, Wijbrans J (2000) New ^{40}Ar/^{39}Ar age of the Bishop Tuff from multiple sites and sediment rate calibration for the Matuyama-Brunhes boundary. J Geophys Res B 105:21431–21443

Sampson DE (1987) Textural heterogeneities and vent area structures in the 600-year-old lavas of the Inyo volcanic chain, eastern California. In: Fink JH (ed) The emplacement of silicic domes and lava flows. Soc Am Spec Pap 212:89–101

Sampson DE, Cameron KL (1987) The geochemistry of the Inyo volcanic chain; multiple magma systems in the Long Valley region, eastern California. J Geophys Res B 92:10403–10421

Schmitt AK, Kasemann S, Meixner A, Rhede D (2002) Boron in central Andean ignimbrites; implications for crustal boron cycles in an active continental margin. Chem Geol 183:333–347

Shaw DM, Sturchio NC (1992) Boron-lithium relationships in rhyolites and associated thermal waters of young silicic calderas, with comments on incompatible element behavior. Geochim Cosmochim Acta 56:3723–3731

Sieh K, Bursik M (1986) Most recent eruption of the Mono Craters, eastern central California. J Geophys Res B 91:12539–12571

Smith BM, Suemnicht GA (1991) Oxygen isotope evidence for past and present hydrothermal regimes of Long Valley Caldera, California. J Volcanol Geotherm Res 48:319–339

Sparks RSJ, Huppert HE, Wilson CJN (1990) Comment on "Evidence for long residence times of rhyolitic magma in the Long Valley magmatic system: the isotopic record in precaldera lavas of Glass Mountain" by Halliday AN, Mahood GA, Holden P, Metz JM, Dempster TJ, Davidson JP. Earth Planet Sci Lett 99:387–389

Spivack AJ, Edmond JM (1987) Boron isotope exchange between seawater and the oceanic crust. Geochim Cosmochim Acta 51:1033–1043

Streck MJ, Grunder AL (1997) Compositional gradients and gaps in high-silica rhyolites of the Rattlesnake Tuff, Oregon. J Petrol 38:133–163

Sturchio NC, Muehlenbachs K, Seitz MG (1986) Element redistribution during hydrothermal alteration of rhyolite in an active geothermal system; Yellowstone drill cores Y-7 and Y-8. Geochim Cosmochim Acta 50:1619–1631

Taylor SR, McLennan SM (1995) The geochemical evolution of the continental crust. Rev Geophys 33:241–265

Tonarini S, Forte C, Petrini R, Ferrara G (2003) Melt/biotite ^{11}B/^{10}B isotopic fractionation and the local environment in the structure of volcanic glasses. Geochim Cosomochim Acta 67:1863–1873

van den Bogaard BP, Schirnick C (1995) ^{40}Ar/^{39}Ar laser probe ages of Bishop Tuff quartz phenocrysts substantiate long-lived silicic magma chamber at Long Valley, United States. Geology 23:759–762

Varga RJ, Bailey RA, Suemnicht GA (1990) Evidence for 600-year-old basalt and magma mixing at Inyo Craters volcanic chain, Long Valley Caldera, California. J Geophys Res B 95:21441–21450

Vogel TA, Eichelberger JC, Younker LW, Schuraytz BC, Horkowitz JP, Stockman HW, Westrich HR (1989) Petrology and emplacement dynamics of intrusive and extrusive rhyolites of Obsidian Dome, Inyo Craters volcanic chain, eastern California. J Geophys Res B 94:17937–17956

Wallace PJ, Anderson AT Jr, Davis AM (1995) Quantification of pre-eruptive exsolved gas contents in silicic magmas. Nature 377:612–616

Wallace PJ, Anderson AT Jr, Davis AM (1999) Gradients in H_2O, CO_2, and exsolved gas in a large-volume silicic magma system; interpreting the record preserved in melt inclusions from the Bishop Tuff. J Geophys Res B104:20097–20122

Watson EB, Harrison TM (1983) Zircon saturation revisited; temperature and composition effects in a variety of crustal magma types. Earth Planet Sci Lett 64:295–304

Webster JD, Holloway JR, Hervig RL (1989) Partitioning of lithophile trace elements between H_2O and $H_2O + CO_2$ fluids and topaz rhyolite melt. Econ Geol 84:116–134

Williams LB, Hervig RL, Holloway JR, Hutcheon I (2001) Boron isotope geochemistry during diagenesis; Part I, Experimental determination of fractionation during illitization of smectite. Geochim Cosmochim Acta 65:1769–1782

Wilson CJN, Hildreth WH (1997) The Bishop Tuff; new insights from eruptive stratigraphy. J Geol 105:407–439